

Article

# Structure of Multipartite Entanglement in Random Cluster-Like Photonic Systems

Mario Arnolfo Ciampini <sup>1,\*</sup> , Paolo Mataloni <sup>1</sup> and Mauro Paternostro <sup>2</sup>

<sup>1</sup> Dipartimento di Fisica, Sapienza Università di Roma, Piazzale Aldo Moro 5, Rome 00185, Italy; paolo.mataloni@uniroma1.it

<sup>2</sup> Centre for Theoretical Atomic, Molecular and Optical Physics, School of Mathematics and Physics, Queen's University Belfast, Belfast BT7 1NN, UK; m.paternostro@qub.ac.uk

\* Correspondence: marioarnolfo.ciampini@uniroma1.it; Tel.: +39-06-4991-3526

Received: 24 July 2017; Accepted: 2 September 2017; Published: 5 September 2017

**Abstract:** Quantum networks are natural scenarios for the communication of information among distributed parties, and the arena of promising schemes for distributed quantum computation. Measurement-based quantum computing is a prominent example of how quantum networking, embodied by the generation of a special class of multipartite states called cluster states, can be used to achieve a powerful paradigm for quantum information processing. Here we analyze randomly generated cluster states in order to address the emergence of correlations as a function of the density of edges in a given underlying graph. We find that the most widespread multipartite entanglement does not correspond to the highest amount of edges in the cluster. We extend the analysis to higher dimensions, finding similar results, which suggest the establishment of small world structures in the entanglement sharing of randomised cluster states, which can be exploited in engineering more efficient quantum information carriers.

**Keywords:** cluster states; multipartite entanglement; percolation

## 1. Introduction

In 1929, the Hungarian author Karinthy famously set out the concept of *six degrees of separation* [1], the conjecture according to which any two living entities on Earth are distant by no more than five intermediate steps. This concept was reprised and developed later on more rigorous sociological and statistical grounds. Remarkably, for instance, a variation of the *six degrees* was unveiled by the group of Barabasi in 1999 [2], who predicted that any page in the World Wide Web can be reached from any other one with only nineteen intermediate steps (or clicks) on average.

As counterintuitive as this result might look, they are actually based on a very solid concept in graph theory, namely the emergence of *small worlds* from connected networks. A small-world network is a type of mathematical graph in which most nodes are not neighbours of one another, but can be reached from every other one by a small number of steps that actually grows logarithmically with the number of nodes themselves. The six and nineteen degrees of separation highlighted above are different yet similar manifestations of the emergence of small worlds in a network.

Can these concepts be exported to the quantum domain? While the theory of quantum networks has found fertile applications in quantum communication [3] and ground-breaking results in the proposal of quantum repeaters for the faithful long-haul transport of quantum information [4,5], the implications of the emergence of small worlds have been far less explored, and mostly confined to studies of excitation-transport and the analysis of the transition from localised to delocalised regimes in spatially extended interacting-particle models [6,7].

Here, inspired by the analogy between classical network bonds and the correlations set between two elements of a given network of quantum particles, we aim at exploring different aspects.

In particular, motivated by the current experimental state-of-the-art in linear optics, which makes available controllable networks of interconnected information carriers, we address the emergence of typical lengths in the entanglement established by a random set of unitary gates applied to the elements of a given graph. In particular, we focus on a particular class of operations and networks, i.e., those typically put in place in the procedure for the creation of so-called cluster states, which are resources for measurement-based quantum computing [8].

Such computational paradigm, which has been demonstrated equivalent to any circuitual quantum computing protocol, is of fundamental importance in quantum information processing. Linear-optics measurement-based quantum information processing has emerged as a promising avenue for the exploration of controllable quantum protocols. Encoding and entangling qubits in more than one degree of freedom of photons is a promising avenue for the generation of medium-to-large scale photonic cluster states: hyperentanglement-based protocols have so far allowed for the creation of cluster states of up to 6 qubits [9], which have been used to validate fundamental one-way quantum algorithms [10,11].

In this paper, by randomising the application of the elementary gates needed to engineer a cluster state of a given size, we induce the establishment of small worlds in the underlying network of a given physical system, and address how the spreading of entanglement across the network itself is affected by the degree of stochasticity of such gates. We unveil an interesting hierarchy with which entanglement appears in subnetworks of growing size: only a sufficient degree of determinism allows for the settling of multipartite entanglement within a given cluster lattice, the threshold for  $k$ -element entanglement depending neatly on the number of elements  $k$  itself. Moreover, we illustrate a fundamental difference between the phenomenology illustrated in this paper and recently introduced concepts of classical entanglement percolation [12].

The significance of this study goes beyond the context set by cluster states and measurement-based quantum information processing and addresses the fundamental concept of entanglement [13]. In fact, the emergence of different lengths at which bipartite and multipartite entanglement emerge from a set of entangling transformations applied to the elements of a given network, provides insightful information on the entanglement sharing structure. In turn, such information could be used to design better resources for quantum information protocols, obtained by applying only a small subset of entangling operations than the whole one determined by the size of the network itself and nevertheless bearing entanglement-sharing properties very close to those of the fully connected network.

The remainder of this paper is organised as follows. In Section 2.1 we present randomly generated cluster states as the platform for our investigation; in Section 2.2 we focus our attention to four-qubit cluster states, presenting a rich analysis on the interplay between stochasticity of the gates used to set the network and the settling of bipartite and multipartite entanglement. In Section 2.3 we extend our analysis to larger networks.

## 2. Results

### 2.1. Theoretical Framework

The approach that we use in order to investigate the core question of our work can be schematised as follows:

1. We set the value of the threshold  $q$  and generate a suitable number of random variables  $p_{ij} \in [0, 1]$ , which embody the probabilities to apply the gate  $\text{CPHASE}_{i,j}(\pi)$  to the pair of qubits  $(e_i, e_j)$ .
2. We compare  $p_{ij}$  to  $q$ . Should it be  $p_{ij} < q$  ( $p_{ij} > q$ ),  $\text{CPHASE}_{i,j}(\pi)$  is (not) applied. We exhaust the number of all inequivalent pairs of qubits in the network. This produces the network state  $|\psi\rangle_\Sigma$ , where  $\Sigma = \{e_1, \dots, e_N\}$  is the set of qubits of the register.
3. We compute the reduced density matrices  $\rho_\sigma = \text{Tr}_{\Sigma \setminus \sigma} [|\psi\rangle\langle\psi|_\Sigma]$  that are obtained upon tracing the overall state over all qubits but those in the subset  $\sigma \in \Sigma$ .
4. We calculate the percent fraction of such reductions that are entangled at the set value of  $q$ .

5. In order to eliminate any dependence on the specific random pattern of applications of the joint gate, we repeat the procedure above for a number  $Q \gg 1$  of instances.
6. When  $Q$  is reached, we change  $q$  and repeat the protocol from point 1 to 5.

Needless to say, the number of applications of  $\text{CPHASE}_{i,j}(\pi)$  at a set value of the threshold depends strongly on the actual value of  $q$  itself: the larger the chosen value of  $q$ , the higher the number of gate applications. This is illustrated in Figure 1, where we show the different configurations achieved for a network of  $N = 8$  elements for  $q = 0.2, 0.5$  and  $1$ , which is associated with a fully connected graph. It is important to remark that, in our notation as well as in Figure 1, a bond connecting elements  $e_i$  and  $e_j$  only means that gate  $\text{CPHASE}_{i,j}(\pi)$  was applied, and does not imply the existence of entanglement between such elements.

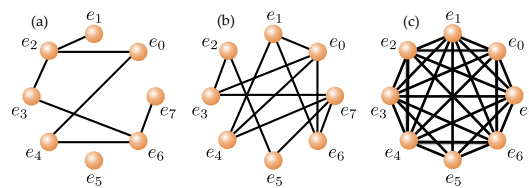


**Figure 1.** Example of instances of an  $N = 8$  qubits random cluster states. For (a–c) we have taken  $q = 0.2, q = 0.5$ , and  $q = 1$  respectively.

Scope of our investigation is ascertaining the phenomenology of distribution of (in general) multipartite entanglement across a given network. In particular, we will focus on the possible emergence of special values of  $q$  that are associated with the onset of multipartite entanglement, and the characterisation of such quantum correlations. The inherently random nature of the resource states that we consider makes any analytical prediction difficult to be drawn and provides the necessary motivations for the statistical approach that, instead, will be used in the analysis that follows. Notwithstanding its limited analytical power, we find such investigation both powerful and insightful.

As a side remark we mention that, as we have in mind a linear-optics implementation, which to date is one of the most promising and successful platforms for the engineering of cluster-state resources, in our analysis we will not account for any effect of dissipation on the random states that are generated using the protocol illustrated above, as photon losses are negligible in such a setting.

## 2.2. Analysis of the Entanglement Structure in a Random Four-Qubit State

We start our analysis by focusing on an intuitive figure of merit that is nevertheless able to provide crucial information on the distribution of entanglement across one of the random graph states discussed above, namely state purity. We thus proceed to compute the purity

$$\mathcal{P}_\sigma = \text{Tr}_\sigma[\rho_\sigma^2] \in [0, 1] \quad (1)$$

of the reduced density matrix  $\rho_\sigma$ , and use the fact that, given the overall pure nature of  $|\psi\rangle_\Sigma$ , a value of  $\mathcal{P}_\sigma < 1$  necessarily implies entanglement in the bipartition  $(\Sigma \setminus \sigma) | \sigma$ . We have thus implemented the protocol illustrated in Section 2.1 by calculating, in step 4, the percentage of reductions with  $\mathcal{P}_\sigma < 1$ .

In order to illustrate the salient features of our analysis, we now address explicitly the case of  $N = 4$ , for which  $\Sigma = \{e_1, \dots, e_4\}$ . The state that would be produced by applying  $\text{CPHASE}_{i,j}(\pi)$  gates to every pair of qubits in the network, which would correspond to choosing  $q = 1$ , reads

$$\begin{aligned}
 |\psi\rangle_{\Sigma} &= \frac{1}{\sqrt{2}} \hat{H}_{e_4} (|\phi_+\rangle_{e_1 e_4} |\phi_-\rangle_{e_2 e_3} + |\psi_+\rangle_{e_1 e_4} |\psi_-\rangle_{e_2 e_3}) \\
 &= \frac{1}{\sqrt{2}} \hat{H}_{e_3} (|\phi_-\rangle_{e_1 e_2} |\phi_+\rangle_{e_3 e_4} - |\psi_+\rangle_{e_1 e_2} |\psi_-\rangle_{e_3 e_4}) \\
 &= \frac{1}{\sqrt{2}} \hat{H}_{e_2} (|\phi_-\rangle_{e_1 e_3} |\phi_+\rangle_{e_2 e_4} - |\psi_+\rangle_{e_1 e_2} |\psi_-\rangle_{e_2 e_4}) \\
 &= \frac{1}{\sqrt{2}} \hat{H}_{e_1} (|\phi_-\rangle_{e_1 e_2} |\phi_+\rangle_{e_3 e_4} - |\psi_+\rangle_{e_1 e_2} |\psi_-\rangle_{e_3 e_4})
 \end{aligned} \tag{2}$$

where  $\hat{H}_{e_j}$  is the Hadamard gate on qubit  $e_j$  and we have introduced the Bell states  $|\phi_{\pm}\rangle_{e_i e_j} = (|00\rangle \pm |11\rangle)_{e_i e_j} / \sqrt{2}$ ,  $|\psi_{\pm}\rangle_{e_i e_j} = (|01\rangle \pm |10\rangle)_{e_i e_j} / \sqrt{2}$ . The orthogonality of Bell states ensures that entanglement exists in the three inequivalent bipartition  $(e_i, e_j)|(e_k, e_l)$ . Moreover, it is equally straightforward to check that any single-qubit reduction is maximally mixed. Therefore, also the bipartitions  $e_i|(e_j, e_k, e_l)$  are entangled. This implies that for  $q = 1$  we expect all six bipartitions that can be identified to be inseparable and the state to be genuinely multipartite entangled. The purity of the associated reduced states is thus necessarily smaller than one. However, for  $q < 1$  the number of mixed-state reduction is not necessarily as large as six, and our calculations aim at quantifying the percentage of such reduced states as  $q$  is varied.

The results of such calculations are presented in Figure 2 (blue and red dots), where each data point is the result of an average over  $Q = 5000$  random instances, a sample-size that was large enough to ensure convergence of the numerics. The error bars attached to each point show the uncertainty associated to the averages, calculated as the standard deviation of each  $Q$ -sized sample and divided by  $\sqrt{Q}$ . Clearly, for  $q = 0$  the state of the network is deterministically found to be the factorised initial state  $\otimes_{j=1}^4 |+\rangle_{e_j}$ , while for  $q = 1$  we retrieve the result anticipated above (Equation (2)). In between such extreme situations, the number of inseparable two-vs.-two and one-vs.-three qubits bipartitions (equivalently, mixed two-qubit and one-qubit states) grows monotonically with  $q$ , albeit at slightly different rates. In particular, we find that the percentage fraction of inseparable two-vs.-two (three-vs.-one) qubits bipartitions exceeds 99.9% at  $q = 0.82 \pm 0.01$  ( $q = 0.89 \pm 0.01$ ), as shown by the vertical dashed line marked as  $T_2$  ( $T_3$ ) in Figure 2. The nominal positions (uncertainties) of  $T_{2,3}$  have been obtained as the average (standard deviations) over 100 analytical non-linear interpolations of the results of our simulations, each producing the functions  $f_{2,3}(q)$  (whose averages are shown by the blue and red lines in Figure 2) that have been used to solve numerically the equations  $f_{2,3}(q) = 99.9$ . Quite clearly,  $T_2 \neq T_3$  beyond statistical errors, which implies that the random network at hand requires a higher threshold in  $q$  to produce a complete set of inseparable one-vs.-three qubits bipartitions.

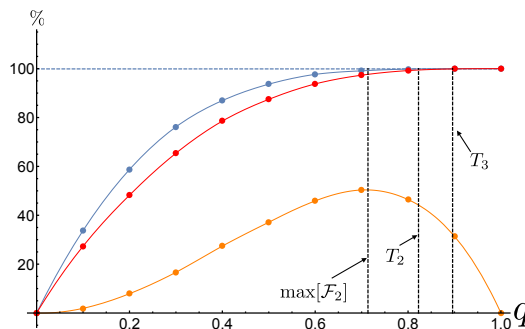


**Figure 2.** We study the percentage fraction of mixed-state reductions that can be identified in a network of  $N = 4$  elements, against the threshold parameter  $q$ . The blue (red) dots show the results of the numerical experiment aimed at quantifying the fraction of mixed two-qubit (one-qubit) reductions. The orange points identify the values of the percentage fraction  $\mathcal{F}_2$  of two-qubit reductions whose purity is exactly  $1/4$ . The solid lines are non-linear interpolations of the data points. Each point is the result of an average over a sample of  $Q = 5000$  elements. Error bars show the standard deviations associated with such averages. Dashed lines  $T_{2,3}$  identify the value of  $q$  at which the number of mixed two- and one-qubit reductions is at least 99.9% of the possible ones. The line labelled  $\max[\mathcal{F}_2]$  identifies the value of  $q$  at which the maximum of  $\mathcal{F}_2$  occurs.

Needless to say, the empirical rule of “no free lunch” applies here as well: the establishment of multipartite entanglement in the network under scrutiny has to come at the expenses of something else, in light of the monogamy of entanglement. The specific algorithm at hand allows us to explore who pays the toll represented by the establishment of genuine multipartite entanglement in the random network.

In particular, we expect bipartite entanglement to be affected by the emergence of multipartite one. Such expectation is corroborated by the analysis summarized by the orange dots and curve in Figure 2, which show the percentage fraction  $\mathcal{F}_2$  of two-vs.-two qubits reductions of random states at a given value of  $q$  that have purity exactly equal to  $1/4$ , which is the lowest a two-qubit state can achieve and witnesses maximum entanglement across the  $(e_i, e_j)|(e_k, e_l)$  bipartition. Quite intuitively,  $\mathcal{F}_2$  grows at small values of  $q$ : a low threshold implies very small probability to apply multiple CPHASE gates, which inevitably favours the construction of maximally entangled two-qubit states. For  $q \simeq 1$ , we have a large probability that one qubit is affected by multiple CPHASE gates. Intuitively, this should be able to set strong multipartite entanglement and deplete the degree of bipartite one, and we expect  $\mathcal{F}_2$  to decrease accordingly. Indeed, we know that at  $q = 1$  we have a genuinely multipartite entangled. The orange dots in Figure 2 confirm such expectation, and show the occurrence of a maximum of  $\mathcal{F}_2$  that is close, yet not identical, to the chosen thresholds  $T_{2,3}$  discussed above (we have that  $\max[\mathcal{F}_2]$  occurs at  $q = 0.72 \pm 0.01$ ).

Of course, counting for the number of reductions that are in mixed states does not provide full information about multipartite nature of the entanglement that is established among the elements of the network. We remind that a pure  $N$ -partite state is called genuinely multipartite entangled if it is not separable with respect to any of the possible bipartitions of its  $N$  elements. One can thus check the multipartite nature of the entanglement of a given pure state by counting the number of separable bipartitions that can be drawn. As each instance of our random sample is a pure state, we have decided to approach this task by using the  $N$ -partite generalisation of negativity defined as

$$\mathcal{E}_N = \sqrt[N]{\prod_{\{\sigma\}} \mathcal{E}_{\sigma|\Sigma \setminus \sigma}} \tag{3}$$

where  $\mathcal{E}_{\sigma|\Sigma\setminus\sigma}$  is the negativity of the partially transposed density matrix of the bipartition  $\sigma|\Sigma\setminus\sigma$  and the product extends to all the bipartitions. We recall the definition of negativity as

$$\mathcal{E}_{\sigma|\Sigma\setminus\sigma} = \max[0, -2 \sum_j \lambda_j^-] \tag{4}$$

with  $\{\lambda_j^-\}$  the set of negative eigenvalues of the partially transposed (with respect to any of the subparties) density matrix of the bipartition  $\sigma|\Sigma\setminus\sigma$ . The geometric average upon which Equation (3) is built is null whenever at least one of the bipartitions of the network is positive under partial transposition. Therefore, for pure states, only if all bipartitions are certified inseparable according to the partial transposition criterion is the state of the network genuinely multipartite entangled. The situation is much more difficult when mixed states are considered, for which the non-nullity of the quantity in Equation (3) is no guarantee of the existence of genuine multipartite entanglement in a given state [14].

Figure 3 shows the behavior of  $\mathcal{E}_4$  against  $q$ . While for  $q > 0$  we always have four-partite entanglement (in line with the finding in Figure 2), it is remarkable that  $q = 1$  is not associated with the largest degree of four-partite negativity, which actually occurs at  $q = 0.72 \pm 0.01$ .

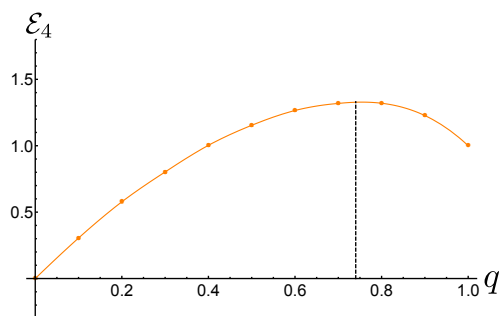


**Figure 3.** Average four-partite negativity  $\mathcal{E}_4$  plotted against  $q$  obtained for a sample of  $Q = 5000$  random network states. The error bars are the standard deviations associated with the averages. The orange solid line is a non-linear interpolating function whose maximum is achieved at  $q = 0.72 \pm 0.01$  (vertical dashed line).

We continue the assessment of the four-partite case by pointing out the differences between the average behavior of the figures of merit addressed herein and the values taken by such indicators over the *average state* of the network. The latter is defined as the state obtained upon mediating over  $Q$  random instances of network states. Formally, by assuming all instances to be equally likely to occur (which is entailed by choosing the probabilities to apply gates  $\text{CPHASE}_{i,j}(\pi)$  uniformly), the physical state of the system is described by the density matrix

$$\rho_\Sigma = \frac{1}{Q} \sum_{j=1}^Q |\psi\rangle\langle\psi|_{\Sigma,j}, \tag{5}$$

where  $|\psi\rangle\langle\psi|_{\Sigma,j}$  is the  $j^{\text{th}}$  random state of the  $Q$ -sized sample.

With the exception of the cases associated with  $q = 0, 1$  (when we sum identically prepared states), by averaging we lose the purity of the network state:  $\mathcal{P}_\Sigma$  reaches values as low as  $\simeq 0.14$  for  $q = 0.5$  (cf. Inset (a) of Figure 4), which is however larger than the minimum purity  $1/16$  achievable by a four-qubit state. Despite being mixed, the average state of the network preserves significant quantum coherences as quantified by the measure proposed in [15] and formalised as

$$\mathcal{C} = \sum_{i \neq j} |(\rho_\Sigma)_{ij}| \tag{6}$$

with  $|(\rho_\Sigma)_{ij}|$  the off-diagonal elements of the density matrix  $\rho_\Sigma$ . The behavior of  $\mathcal{C}$  against  $q$  is shown in Inset (b) in Figure 4: a minimum of the measure of coherence is achieved in correspondence of the minimum purity. However, such a minimum is strictly non-null, thus leaving open the possibility of dealing with a (mixed) state of the network exhibiting a non-trivial entanglement structure. Such a possibility is confirmed by the analysis of  $\mathcal{E}_4$  (cf. main panel of Figure 4), which is a growing function of  $q$  (similar trends are exhibited by both the two-vs.-two qubits entanglement  $\mathcal{E}_{(e_i, e_j)|(e_k, e_l)}$ , and the one-vs.-three qubits one  $\mathcal{E}_{(e_i)|(e_j, e_k, e_l)}$ ). Nothing remarkable in the behavior of  $\mathcal{E}_4$  appears to be related to the value of  $q = 0.5$ , although the function changes concavity in correspondence to such a value of the probability threshold. It should be noticed that, as anticipated, in such an average-state case  $\mathcal{E}_N$  cannot be interpreted as a quantifier of genuine multipartite entanglement. Indeed, the revelation of multipartite entanglement in general multiparty mixed states requires a more refined approach (see [16] for a recent assessment of this point and the provision of useful criteria). Nevertheless, this figure of merit is still very useful for our analysis, as it provides valuable information on the average amount of bipartite entanglement within the statistically average stage of the network, and we will thus make further use of  $\mathcal{E}_N$  in the remainder of this work. Finally, the non-nullity of either  $\mathcal{E}_{(e_i)|(e_j, e_k, e_l)}$ 's or  $\mathcal{E}_{(e_i, e_j)|(e_k, e_l)}$ 's does not exclude the possibility of facing bound entanglement (i.e., non-distillable entanglement) of the negative-partial-transposition nature [17] in those bipartitions, an issue that goes beyond the scopes of this work.

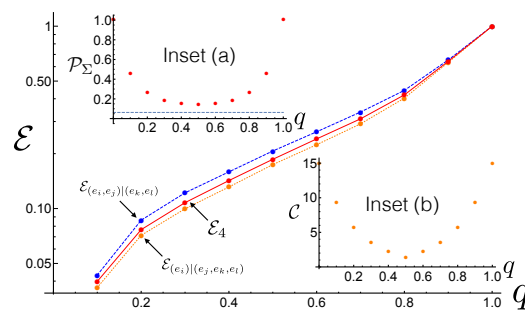


**Figure 4.** Main panel: Logarithmic plot of the entanglement within the average estate  $\rho_\Sigma$  of an  $N = 4$  random network against the threshold probability  $q$ . The red dots show the value taken by the four-partite negativity  $\mathcal{E}_4$ , while the blue and orange ones are for the entanglement within the bipartitions  $(e_i, e_j)|(e_k, e_l)$  and  $(e_i)|(e_j, e_k, e_l)$ . The lines connecting the dots are simply guides to the eye. Inset (a): Purity  $\mathcal{P}_\Sigma$  of the average state against  $q$ . The dashed horizontal line shows the minimum purity of a four-qubit state. Inset (b): Values taken by the measure of coherence  $\mathcal{C}$  against the threshold probability.

To finish the study of this paradigmatic case, we report in the main panel of Figure 5 the behavior of  $\mathcal{E}_3$  in the four three-qubit reduced states that can be singled out from our network. We have used the tripartite version of Equation (3) to quantify the entanglement and changed our notation so as to make explicit the triplets of elements of the network that we have considered. Moreover, by tracing out two elements, we have evaluated the residual two-qubit entanglement, whose average across the six two-qubit reductions is displayed in the inset of Figure 5. The general trend of such figures of merit follows the expectation that, in the large- $q$  region, the entanglement in the reduction is depleted to favour the emergence of multipartite one. Moreover, their quantitative value is, in general, very small. A point of notice is that the peak of three- and two-qubit negativity does not occur at the same value of  $q$ , thus suggesting an interesting hierarchy of values of  $q$  at which the various structures of entanglement across the system are triggered or destroyed.

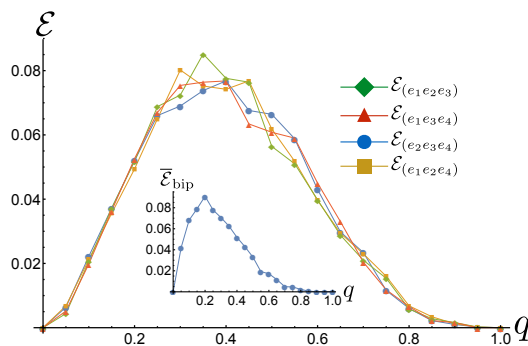


**Figure 5.** Main panel:  $\mathcal{E}_3$  in the three-qubit reductions (extracted from an  $N = 4$  network) identified in the legend, plotted against  $q$ . Each plot is an average over  $Q = 5000$  realisation of the random network state (we omit the error bars for clarity of presentation). Inset: Mean bipartite negativity  $\bar{\mathcal{E}}_{\text{bip}}$  averaged over the six two-qubit reduced states that can be singled out from our network. Same conditions as in the main panel.

### 2.3. Enlarging the Size of the Network

We now assess the features of larger networks of qubits, addressing questions that are akin to those assessed in Section 2.2. Features similar to those showcased in the four-qubit network are present in all the higher-dimensional systems that we have studied through our simulations. For instance, Figures 6 and 7 display the same behaviors highlighted in Figures 2 and 4, respectively. Rather than reporting qualitatively similar plots for larger networks, in Table 1 we present the threshold values of  $q$  at which progressively larger reductions of the state of the network are mixed.

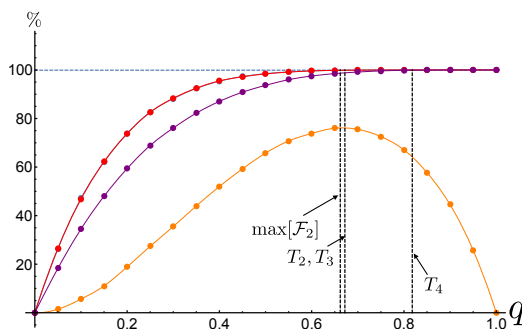


**Figure 6.** We study the percentage fraction of mixed-state reductions that can be identified in a network of  $N = 5$  elements, against the threshold parameter  $q$ . The red dots show the results of the numerical experiment aimed at quantifying the fraction of mixed two- and three-qubit reductions, which actually coincide. The purple dots show the results for the one-qubit reductions. The orange points identify the values of the percentage fraction  $\mathcal{F}_2$  of two-qubit reductions whose purity is exactly  $1/4$ . The solid lines are non-linear interpolations of the data points. Each point is the result of an average over a sample of  $Q = 10^4$  elements. Error bars show the standard deviations associated with such averages. Dashed lines  $T_{2,3}$  ( $T_4$ ) identify the value of  $q$  at which the number of mixed two- and three-qubit (one-qubit) reductions is at least 99.9% of the possible ones. The line labelled  $\max[\mathcal{F}_2]$  identifies the value of  $q$  at which the maximum of  $\mathcal{F}_2$  occurs.

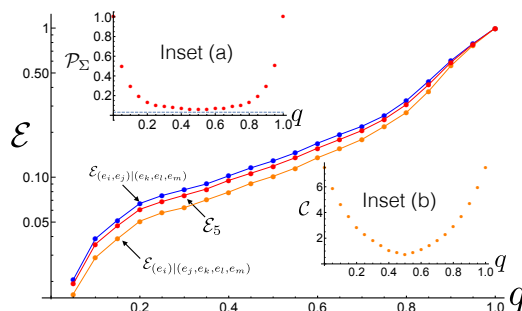


**Figure 7.** Main panel: Logarithmic plot of the entanglement within the average estate  $\rho_\Sigma$  of an  $N = 5$  random network against the threshold probability  $q$ . The red dots show the value taken by  $\mathcal{E}_5$ , while the blue and orange ones are for the entanglement within the bipartitions  $(e_i, e_j)|(e_k, e_l, e_m)$  and  $(e_i)|(e_j, e_k, e_l, e_m)$ . The lines connecting the dots are simply guides to the eye. Inset (a): Purity  $\mathcal{P}_\Sigma$  of the average state against  $q$ . The dashed horizontal line shows the minimum purity of a four-qubit state. Inset (b): Values taken by the measure of coherence  $\mathcal{C}$  against the threshold probability.

The trend is clear: as we look into larger networks, the value of  $T_k$  ( $k = 2, 3, \dots$ ) decreases.

**Table 1.** The table shows the threshold value of  $q$  at which the fraction of progressively larger reductions in an  $N$ -element random network is at least 99.9%. Black squares stands for unavailable data at that size of the network. As before,  $\max[\mathcal{F}_2]$  is the value of  $q$  at which the maximum of  $\mathcal{F}_2$  occurs.

<b>N</b>	4	5	6	...	9
$\max \mathcal{F}_2$	0.72	0.66	0.64		0.40
$T_2$	0.82	0.67	0.57		0.39
$T_3$	0.89	0.67	0.54		0.31
$T_4$	■	0.818	0.57		0.27
$T_5$	■	■	0.75		0.27
$T_6$	■	■	■		0.31
$T_7$	■	■	■		0.39
$T_8$	■	■	■		0.40

### 2.4. Entanglement Percolation

It is interesting to compare our analysis to entanglement percolation, a concept akin to classical bond percolation introduced in [12]. Consider a graph of particles akin to one of those addressed in this paper. This time, though, a link between two elements implies the presence of entanglement between them. Ref. [12] shows the existence of a minimum amount of entanglement between any two elements of the network needed to establish a perfect quantum channel between distant (not directly connected) elements, with significant (non-exponentially decaying) probability.

This is fundamentally different from our situation, where instead we point out the existence of a minimum probability to randomly apply a two-qubit gate in a network associated with the establishment of a genuinely multipartite entangled state of the network. Our threshold does not guarantee the existence of a long-distance entangled channel between arbitrarily chosen elements of the network. In fact, non-nearest-neighbour elements of a cluster state are not necessarily entangled, their entanglement being in general dependent on the geometry of the underlying network.

In order to ascertain if a value of  $q$  exists above which long-haul entanglement is set in the network, we computed the negativity of the reduced state of the qubits that have the largest number of intermediate sites between them, at a given value of  $N$ . This is analogous to the study presented in the inset of Figure 5, although instead of an average over all the possible two-qubit reductions, here we consider now only a specific reduction. Figure 8 shows the results valid for the case of  $N = 6$ , for which we address the entanglement between elements  $e_1$  and  $e_4$ . We have considered the percentage of reductions of such elements with a non-zero value of negativity against the value of  $q$ . Quite clearly,

such a percentage remains always very small, regardless of  $q$ , showing that no classical entanglement percolation effect occurs, as there is no value of  $q$  at which long-distance entanglement within the network is set deterministically. The results should be considered as canonical, qualitatively valid regardless of the actual choice of  $N$ , and indicative of the profound differences between the situation addressed here and the study in [12].

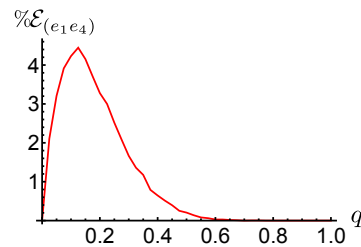


**Figure 8.** Percentage of reduced states of elements  $e_1$  and  $e_4$  of an  $N = 6$  random network exhibiting a non-zero negativity, plotted against  $q$ , for a sample of  $5 \times 10^4$  states.

### 3. Discussion

We have studied the entanglement sharing structure among the elements of a qubit network subjected to probabilistic CPHASE gates. We have highlighted the existence of statistically inequivalent thresholds in the probability of application of the gates for the settling of entanglement in various subsets of network elements, thus unveiling an interesting hierarchy in the entanglement distribution pattern of a given network. The phenomenology that we have highlighted cannot be understood in terms of the statistical properties of an intuitive, yet too naive, reference state such as the one obtained by averaging overall the elements of the random set of states generated in our numerical experiments: the above-mentioned hierarchy is a statistical feature of random networks rather than a property of the statistically average state of the network. Remarkably, *small worlds* structures in the entanglement sharing of the random set of network states appear to emerge. This is an interesting feature that deserves more attention and upon which we plan to focus our forthcoming (theoretical and experimental) efforts.

**Acknowledgments:** Mario Arnolfo Ciampini acknowledges support from QUCHIP-Quantum Simulation on a Photonic Chip, FETPROACT-3-2014, Grant agreement no: 641039, Mauro Paternostro acknowledges support from the SFI-DfE Investigator Programme (grant 15/IA/2864), and the Royal Society.

**Author Contributions:** Mario Arnolfo Ciampini conceived the idea, Mario Arnolfo Ciampini and Mauro Paternostro performed the simulation and analysed the data, Mauro Paternostro and Paolo Mataloni interpreted the results, all authors contributed to drafting and revising the manuscript.

**Conflicts of Interest:** The authors declare no conflict of interest.

### References

1. Karinthy, F. Láncszemek. In *Minden Masképpen van*, 1929. Available online: <http://mek.oszk.hu/15500/15588/15588.pdf> (accessed on 5 September 2017). (In Hungarian)
2. Albert, R.; Jeong, H.; Barabasi, A.-L. Internet: Diameter of the World-Wide Web. *Nature* **1999**, *401*, 130–131.
3. Kimble, H.J. The quantum internet. *Nature* **2008**, *453*, 1023–1030.
4. Munro, W.J.; Harrison, K.A.; Stephens, A.M.; Devitt, S.J.; Nemoto, K. From quantum multiplexing to high-performance quantum networking. *Nat. Photonics* **2010**, *4*, 792–796.
5. Epping, M.; Kampermann, H.; Bruß, D. Robust entanglement distribution via quantum network coding. *New J. Phys.* **2016**, *18*, 103052.
6. Zhu, C. P.; Xiong, S.-J. Localization-delocalization transition of electron states in a disordered quantum small-world network. *Phys. Rev. B* **2000**, *62*, 14780.
7. Giraud, O.; Georgeot, B.; Shepelyansky, D.L. Tuning clustering in random networks with arbitrary degree distributions. *Phys. Rev. E* **2005**, *72*, 036203.

8. Briegel, H.J.; Browne, D.E.; Dür, W.; Raussendorf, R.; Van den Nest, M. Measurement-based quantum computation. *Nat. Phys.* **2009**, *5*, 19.
9. Vallone, G.; Donati, G.; Ceccarelli, R.; Mataloni, P. Six-qubit two-photon hyperentangled cluster states: Characterization and application to quantum computation. *Phys. Rev. A* **2010**, *81*, 052301
10. Vallone, G.; Pomarico, E.; De Martini, F.; Mataloni, P. One-way quantum computation with two-photon multiqubit cluster states. *Phys. Rev. A* **2008**, *78*, 042335.
11. Ciampini, M.A.; Orioux, A.; Paesani, S.; Sciarrino, F.; Corrielli, G.; Crespi, A.; Ramponi, R.; Osellame, R.; Mataloni, P. Path-polarization hyperentangled and cluster states of photons on a chip. *Light Sci. Appl.* **2016**, *5*, e16064.
12. Acín, A.; Cirac, J.I.; Lewenstein, M. Entanglement Percolation in Quantum Networks. *Nat. Phys.* **2007**, *3*, 256.
13. Horodecki, R.; Horodecki, P.; Horodecki, M.; Horodecki, K. Quantum entanglement. *Rev. Mod. Phys.* **2009**, *81*, 865.
14. Huber, M.; Mintert, F.; Gabriel, A.; Hiesmayr, B.C. Detection of high-dimensional genuine multipartite entanglement of mixed states. *Phys. Rev. Lett.* **2010**, *104*, 210501.
15. Baumgratz, T.; Cramer, M.; Plenio, M.B. Quantifying Coherence. *Phys. Rev. Lett.* **2014**, *113*, 140401.
16. Lancien, C.; Gühne, O.; Sengupta, R.; Huber, M. Relaxations of separability in multipartite systems: Semidefinite programs, witnesses and volumes. *J. Phys. A Math. Theor.* **2015**, *48*, 505302.
17. Horodecki, P.; Horodecki, R. Distillation and bound entanglement. *Quant. Inf. Comp.* **2001**, *1*, 45.



© 2017 by the authors. Licensee MDPI, Basel, Switzerland. This article is an open access article distributed under the terms and conditions of the Creative Commons Attribution (CC BY) license (<http://creativecommons.org/licenses/by/4.0/>).